Exp Fluids (2007) 42:403–411
DOI 10.1007/s00348-006-0247-1

RESEARCH ARTICLE

Comparison of CCD, CMOS and intensified cameras

Rainer Hain · Christian J. Kähler · Cam Tropea

Received: 15 August 2006 / Revised: 16 November 2006 / Accepted: 6 December 2006 / Published online: 13 January 2007
© Springer-Verlag 2007

Abstract The properties of digital cameras are often important to obtain accurate results with image based measurement techniques. Unfortunately, a detailed comparison of the sensor specifications and performance is not accessible as this information is normally not provided by the manufacturers and no generally accepted comparison standard exists. Therefore, a detailed quantitative comparison was performed to evaluate and assess the characteristics of state-of-the-art CCD, CMOS and intensified CMOS sensors. These results may be of assistance when selecting the appropriate sensor for a desired application.

1 Introduction

Digital cameras are increasingly applied to conveniently and reliably measure a physical quantity at multiple points simultaneously. In fluid mechanics, for instance, the following techniques are typical examples: particle image velocimetry (PIV), particle tracking velocimetry (PTV), molecular tagging velocimetry (MTV), Doppler global velocimetry (DGV), pressure sensitive paint (PSP), infrared (IR) thermography, background oriented schlieren (BOS), conventional schlieren and shadow graph methods, and direct visualization. For purely qualitative investigations, the properties of the sensors are usually less important. However, when a quantitative evaluation of the data is required, the measurement results are more or less affected by the recording medium, whether interest is in the locations of tiny weak bright objects (as in PIV, PTV and BOS) or the precise magnitude of the accumulated gray value (as in DGV, PSP and IR-thermography).

The basic properties of the sensors are quite complex (Theuwissen 1995; Janesick 2001; Jähne 2004). For example, the sensitivity of a pixel is given by the quantum efficiency, defined as the number of generated electrons per photon of a given frequency. This value depends mainly on the spectral photon absorption line in silicon, on the thickness of the impoverishment-layer, on the thickness and reflectivity of the metal-oxide layer the photon must pass before it may generate an electron-hole pair, on the fill ratio of the pixel, and finally, on the diffusion-length of the electrons in the silicon which contribute to the signal (Strüder and von Zanthier 1998). However, only the integral value is of interest for the above mentioned measurement techniques (European machine vision 2005). For this reason, the following discussion will examine the sensitivity, linearity, signal-to-noise ratio (SNR), and image uniformity. Table 1 lists the examined CCD and CMOS cameras (http://www.DantecDynamics.com; http://www.LaVision.de; http://www.LMT-Berlin.de; http://www.PCO.de;

R. Hain (✉) · C. J. Kähler
Institut für Strömungsmechanik,
Technische Universität Braunschweig,
Bienroder Weg 3, 38106 Braunschweig, Germany
e-mail: r.hain@tu-bs.de

C. J. Kähler
e-mail: c.kaehler@tu-bs.de

C. Tropea
Fachgebiet Strömungslehre und Aerodynamik,
Technische Universität Darmstadt,
Petersenstraße 30, 64287 Darmstadt, Germany
e-mail: ctropea@sla.tu-darmstadt.de

Table 1 Specifications of the cameras investigated

Camera	Resolution (px^2)	Pixelsize (μm^2)	fps (1/s)	*IF* (ns)
PCO Sensicam[a,d]	1,280 × 1,024	6.7 × 6.7	8	300
DantecDynamics NanoSense MKIII[b]	1,280 × 1,024	12 × 12	1,024	100
DantecDynamics iNanoSense MK7[c,f]	1,280 × 1,024	12 × 12	1,024	100[e]
PCO 1200hs[b]	1,280 × 1,024	12 × 12	638	75
Photron APX[b]	1,024 × 1,024	17 × 17	2,000	2000
Photron APX-i2[c]	1,024 × 1,024	17 × 17	2,000	2000[e]
Redlake HG 100K[b]	1,504 × 1,128	12 × 12	1,000	3000

Restriction due to data given in Table 2

fps frames per second

IF interframe time

[a] CCD

[b] CMOS

[c] Intensified CMOS

[d] This camera is indentical with the LaVision Flowmaster3S

[e] CMOS interframe time

[f] This camera is identical with the IDT XS5-i

Table 2 Specifications of the image intensifiers

Camera	Resolution (lppm[a])	minimum gate time (ns)	phosphor decay time (μs)
DantecDynamics iNanoSense MK7	64	50	≈ 5
Photron APX-i2	28	20	≈ 10

[a] Line pairs per mm

http://www.Photron.com; http://www.Redlake.com; http://www.idtpiv.com) and Table 2 summarizes additional information for the intensified CMOS systems.

2 Experimental setup

In order to determine the aforementioned characteristics of a camera, the experimental setup displayed in Fig. 1 was employed. The illumination of the sensor was performed with a white light LN3 luminance standard, called an Ulbricht sphere, from LMT Lichtmesstechnik GmbH Berlin, with an aperture of 70 mm (http://www.LMT-Berlin.de). The Ulbricht sphere emits a well-defined intensity homogeneously over the entire aperture. The device is controlled in such a way that the luminance at the diffusing screen is constant at L = 1,063 cd/m^2. The correlated color temperature is T_n = 2,855 K. The camera sensor is directly illuminated by the Ulbricht sphere without any lens. In contrast to the EMVA 1288 standard (European machine vision 2005), here the illumination strength on the sensor was varied by changing the distance d between the Ulbricht sphere and the sensor. Therefore, the camera was mounted on a linear translation stage to adjust the distance, d (smallest $d \approx 0.18$ m; largest $d \approx 1.5$–5 m), with an accuracy better than 0.5 mm. The exposure time of the camera sensor was constant for all distances. For the CCD sensor, the exposure time was chosen in such a way that the smear effect did not affect the results.

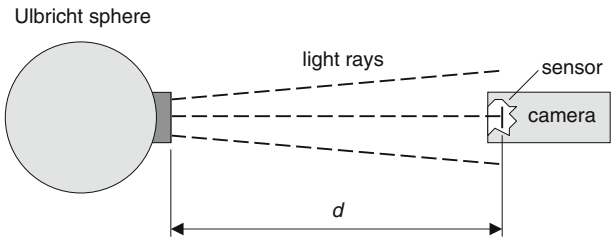


Fig. 1 Principle setup of the camera test

3 Evaluation

The illuminance, E_{sensor}, at the position of the sensor is calculated using the Eq. 1:

$$E_{sensor} = \frac{\pi \cdot r^2}{r^2 + d^2} L \tag{1}$$

where r is the radius of the diffusing screen of the Ulbricht sphere, d is the distance shown in Fig. 1, and L is the luminance of the Ulbricht sphere at the diffusing screen. There are mainly two values dependent on E_{sensor} which must be determined: the signal, S, and the noise, N. For the evaluation, a rectangular subregion (100 × 100 px^2) of the image (without pixel defects or artifacts) was considered.

In the following derivation, $G_k(x, y)$ is the normalized gray value of image k at pixel position x, y. The normalization is performed with the maximum gray value (255 for an 8 bit image). $G_{dark,k}$ (x, y) is the normalized gray value of pixel x, y of the dark image k. The dark image is an image without any illumination (covered sensor).

3.1 Calculation of the signal, S

With the definitions given above, S is calculated by means of Eq. 2 for the selected rectangle (from x_{start} to x_{end} and from y_{start} to y_{end}) for K_S images.

$$S = \sum_{x=x_{start}}^{x_{end}} \sum_{y=y_{start}}^{y_{end}} \sum_{k=1}^{K_S} \frac{G_k(x,y) - G_{dark,k}(x,y)}{I}. \tag{2}$$

The total number of pixels, I, is calculated by

$$I = (x_{\text{end}} - x_{\text{start}} + 1) \cdot (y_{\text{end}} - y_{\text{start}} + 1) \cdot K_S. \quad (3)$$

By subtracting the normalized gray values of the dark images, the dark current is removed and only the normalized signal remains, provided that the temporal variation of the dark current is negligible. K_S was set to 10.

3.2 Calculation of the noise, N

For the calculation of N, the same rectangle is considered as for the calculation of S. A fixed pattern noise and a variation of the mean gray value from one image to the next image should not have an influence on the noise. Therefore, the calculation is performed in the following way. Matrix M is used as a temporary matrix with the coefficients $M_k(x, y)$.

$$M_k(x,y) = [G_{2\cdot k}(x,y) - G_{2\cdot k-1}(x,y) - (G_{\text{mean},2\cdot k} - G_{\text{mean},2\cdot k-1})]\big|_{x=x_{\text{start}}}^{x_{\text{end}}}\big|_{y=y_{\text{start}}}^{y_{\text{end}}}\big|_{k=1}^{K_N}. \quad (4)$$

The mean gray value $G_{\text{mean},k}$ of image k is calculated by

$$G_{\text{mean},k} = \sum_{x=x_{\text{start}}}^{x_{\text{end}}} \sum_{y=y_{\text{start}}}^{y_{\text{end}}} \frac{G_k(x,y)}{(x_{\text{end}} - x_{\text{start}} + 1) \cdot (y_{\text{end}} - y_{\text{start}} + 1)}. \quad (5)$$

By subtracting the gray values $[G_{2\cdot k}(x, y) - G_{2\cdot k-1}(x, y)]$, the influence of a fixed pattern noise on the calculation of N is avoided. Subtracting $G_{\text{mean},\,2\cdot k}$–$G_{\text{mean},\,2\cdot k\,-\,1}$ in Eq. 4 avoids an influence of the varying image intensity from one image to the next image on the noise. N is now calculated by

$$N = \frac{1}{\sqrt{2}} \cdot \sqrt{\frac{\sum_{x=x_{\text{start}}}^{x_{\text{end}}} \sum_{y=y_{\text{start}}}^{y_{\text{end}}} \sum_{k=1}^{K_N} \left[M_k^2(x,y)\right]}{(x_{\text{end}} - x_{\text{start}} + 1) \cdot (y_{\text{end}} - y_{\text{start}} + 1) \cdot K_N - 1}}. \quad (6)$$

K_N was set to 5 so that 10 images were used to calculate the noise, similar to the calculation of the signal.

4 Results

In the subsequent discussion, the dependence of different quantities on the illuminance, E_{sensor}, multiplied by the exposure time, Δt, is shown. This product is proportional to the number of impinging photons. For many experiments where lasers are applied, the same situation occurs because the amount of light (number of photons) is given by the pulse energy. For measurement techniques which use a continuous light source, a short exposure time of the camera is required in order to avoid motion blur. Therefore, the exposure time is given in the graphs. The following points are essential when examining the figures below:

- The graphs of the PCO Sensicam end at relative high $E_{\text{sensor}}\cdot\Delta t$. This is due to the experimental setup which did not allow larger distances between the Ulbricht sphere and the sensor. In addition, the exposure time could not be reduced in order to avoid an influence of the smear effect on the results. We can assume that the graphs of the Sensicam can be extrapolated to lower $E_{\text{sensor}}\cdot\Delta t$.
- In the case of the Photron APX cameras, the dark images were directly subtracted during the experiments. This leads to gray values becoming zero when the illumination is small. In that case, the signal and the noise cannot be calculated in the correct manner. The Redlake cameras also show this effect at low illuminations.
- The gains of the intensifiers of the DantecDynamics iNanoSense MK7 and of the Photron APX-i2 are adjustable. In case of a decreasing illumination the gain can be increased to increase the signal. This was not done here because the resulting graphs would not provide any additional information. In order to compare both cameras, a similar exposure time and a nearly similar gain of the intensifiers was chosen.
- The graphs of the PCO 1200hs show some peaks. These peaks result from gray values which cannot be read out due to design flaws of the Micron CMOS image sensor which is used in this camera.
- The DantecDynamics, Photron and Redlake cameras offer 8 bit images. The internal dynamic of the cameras is higher so that the gray values are mapped on a scale from 0 to 255. For the DantecDynamics cameras only the lower 8 bits are read out and mapped on the 8 bit image (the software does not allow mapping the full dynamic range on an 8 bit image). In the case of the Photron cameras, the full internal dynamic range is mapped on an 8 bit image for all results given in this paper. Two graphs are shown for the Redlake cameras. One graph shows the results where the lower internal 8 bits are read out and written in an 8 bit image. The other graphs reveal the results where the internal 12 bits are mapped linearly on an 8 bit image. For real applications, the user can create a look-up-table.

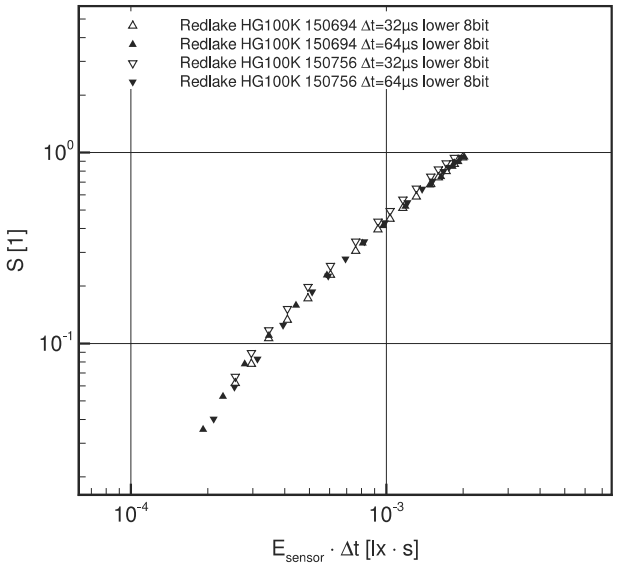


Fig. 2 Dependence of the signal, S, on $E_{sensor}{\cdot}\Delta t$ for two Redlake HG100K cameras each with two exposure times

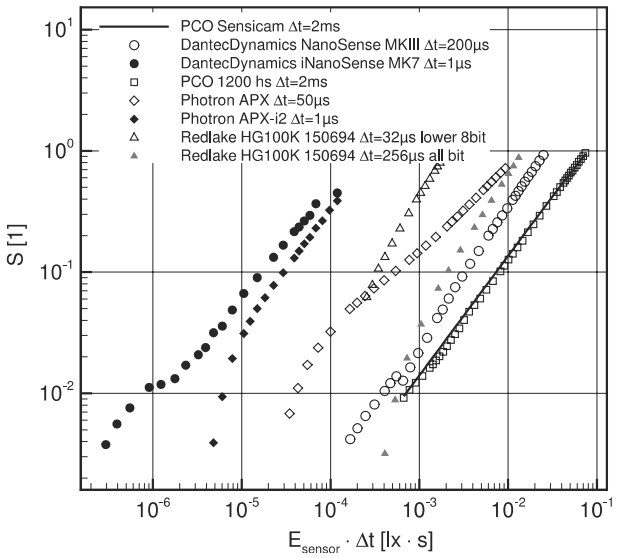


Fig. 3 Dependence of S on $E_{sensor}{\cdot}\Delta t$

– Due to the different sensor sensitivities and camera gains (given by the manufacturer), it was not possible to use the same exposure time for all cameras. In order to exclude an effect of the exposure time on the results, all measurements have been done with two identical Redlake HG100K cameras, each at two exposure times. One example of the results is shown in Fig. 2. The agreement of the four graphs indicate that the influence of the exposure time is negligible. In all other figures, only one graph of the Redlake cameras is shown for a better clarity.

In the following figures, the results of the PCO Sensicam, being the only shown CCD camera, are displayed by means of a solid line. The two intensified cameras from DantecDynamics and Photron can be identified by the **i** in their name (**i**NanoSense MK7 and APX-**i**2).

4.1 Linearity

The camera signal should depend linearly on the product $E_{sensor}{\cdot}\Delta t$. Figure 3 illustrates that all sensors are quite linear over a wide range (the points where saturation takes place are not shown). The linear range covers two orders of magnitude in the case of the CCD sensor (PCO Sensicam). In the case of the CMOS sensors, non-linear effects can only be observed at lower intensities. By comparing the Photron APX with the APX-i2 or the DantecDynamics NanoSense MKIII with the intensified iNanoSense MK7 camera, the figure shows the gain in sensitivity that can be obtained by using the intensified camera version. The different gradient is a result of the difference in gain between the pure sensor and the intensifier.

The graph of the NanoSense MKIII shows an abrupt step at $(E_{sensor}{\cdot}\Delta t) \approx 6{\cdot}10^{-4}$ lx·s. To explain this, the dependence of the normalized mean gray value of 20 images over a rectangular subsection (100×100 px^2) on the elapsed time after switching on the camera is shown in Fig. 4. It can be observed that the mean gray

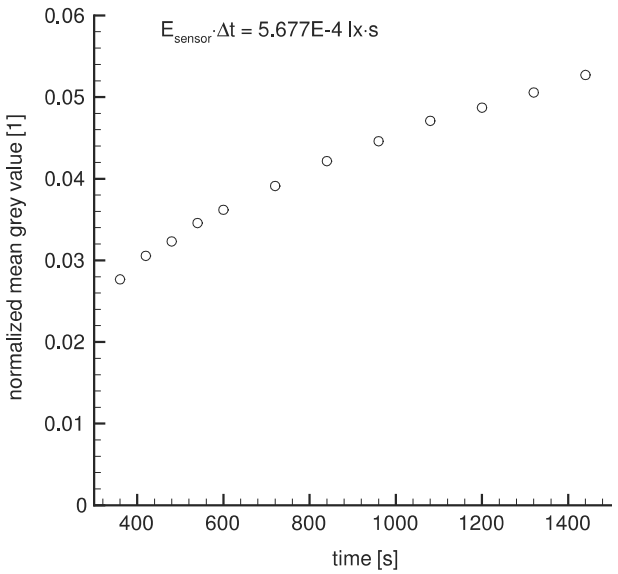


Fig. 4 Dependence of the normalized mean gray value on the elapsed time after switching on the camera (DantecDynamics MKIII, no dark image subtracted, $E_{sensor}{\cdot}\Delta t = 5.677{\cdot}10^{-4}$ lx·s)

value increases with increasing time. When performing the experiment for Fig. 3, the camera was traversed on a linear translation stage from a position near the Ulbricht sphere to positions farther away (the time for moving the camera from one position to the next position was approximately 30 s). At the position where the step occurs, the whole linear translation stage was repositioned in order to realize larger distances between the sensor and the Ulbricht sphere. The alignment after moving took a few minutes so that the mean gray value increased, according to Fig. 4.

4.2 Signal-to-noise ratio (SNR)

The SNR is the essential measure of the image quality. The goal is a high SNR, such that the influence of the camera noise on the measurement is small. The SNR is the ratio of Eqs. 2 and 6, according to Sects. 3.1 and 3.2. Figure 5 shows the dependence of the SNR on $E_{\text{sensor}}\cdot\Delta t$ for the different sensors examined here. In comparison with the CCD camera, the CMOS cameras have a relatively high SNR. The reason is the large pixel size of the CMOS sensors which normally leads to a higher full well capacity (under consideration of the fill factor). The intensified cameras offer a relative high SNR at very low illuminations, which means that measurements can be performed with low illumination or laser power. As mentioned previously, the graphs of the Redlake camera and the graphs of the Photron cameras are erroneous in the lower regions due to the fact that many pixels have gray values of zero counts. The dependence of the SNR on the signal, S, is given in Fig. 6 in order to simplify the assessment of the SNR

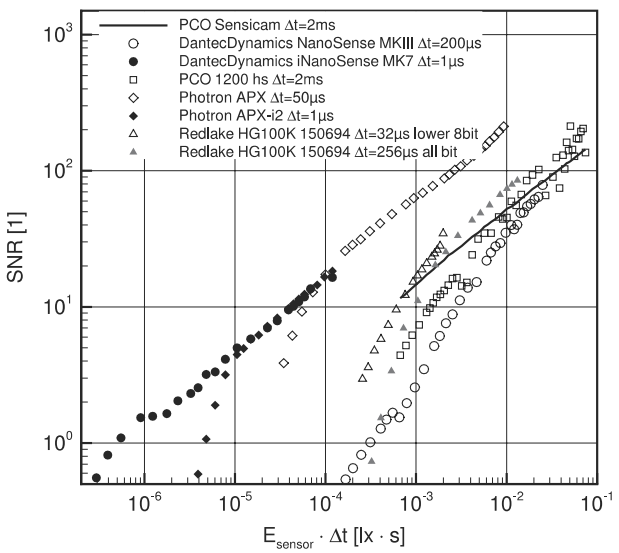


Fig. 5 Dependence of the SNR on $E_{\text{sensor}}\cdot\Delta t$

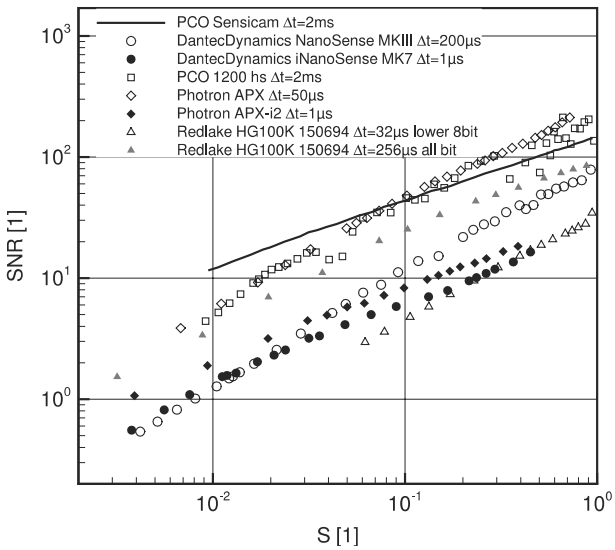


Fig. 6 Dependence of the SNR on S

for a given signal. It can be seen that the Photron APX, the PCO 1200 hs, and the PCO Sensicam offer quite high SNR at high signals. For the intensified cameras, the SNR is much smaller. All experiments have been performed at room temperature. Scientific CCD sensors are usually cooled in order to reduce the dark current noise N_{d} which is proportional to $\sqrt{\text{dark current}}$. The dark current increases proportionally with the exposure time and decreases exponentially with the sensor temperature (the dark current is halved every ≈7 K the sensor is cooled down (StrüderStrüder and von Zanthier 1998). A reduction of the sensor temperature by 14 K, for instance, decreases the dark current noise by a factor of 2. Especially for longer exposure times, the sensor cooling is an appropriate possibility to reduce noise.

4.3 Image uniformity

The images should be as uniform as possible. Usually, dark images are subtracted from the recorded images when measuring with CMOS cameras to improve the image uniformity (removing fixed pattern noise). In order to quantify the image uniformity, 20 images for each camera and every $E_{\text{sensor}}\cdot\Delta t$ were considered. The average, $G_{\text{mean}}(x,y)$, was calculated from these 20 images. The same procedure was done for 20 dark images, resulting in $G_{\text{dark, mean}}(x,y)$. The averaged images were subtracted so that only the signal remained. The averaging leads to a reduction of the temporal noise. An approximation (temporal noise is not fully avoided) for the spatial standard deviation, σ_{spatial}, is calculated by Eq. 7:

$$
\begin{aligned}
G_{\text{mean}}(x,y) &= \sum_{k=1}^{K_U} \frac{G_{\text{k}}(x,y)}{K_U} \\
G_{\text{dark,mean}}(x,y) &= \sum_{k=1}^{K_U} \frac{G_{\text{dark,k}}(x,y)}{K_U} \\
S_{\text{unif}}(x,y) &= G_{\text{mean}}(x,y) - G_{\text{dark,mean}}(x,y) \\
S_{\text{unif}} &= \frac{\sum_{x=1}^{I_x}\sum_{y=1}^{I_y}(S_{\text{unif}}(x,y))}{I_x \cdot I_y} \\
\sigma_{\text{spatial}} &= \sqrt{\frac{\sum_{x=1}^{I_x}\sum_{y=1}^{I_y}(S_{\text{unif}}(x,y) - S_{\text{unif}})^2}{I_x \cdot I_y - 1}}
\end{aligned}
\tag{7}
$$

with $K_U = 20$ being the number of images used for the calculations. I_x and I_y are the number of pixels of an image in x- and y- direction. S_{unif} is nearly similar to the signal, S, calculated above. In opposition to S, the entire image is considered for calculating S_{unif}. The result is shown in Fig. 7. It can be observed that the PCO Sensicam has the best image uniformity. For high signals, the PCO 1200hs and the Photron APX also offer quite good uniformities. In Fig. 8 lineplots for $x = I_x/2$ are given to highlight the CCD response performance. The image uniformity of the intensified cameras is analyzed in more detail as follows. Exemplary images for both intensified cameras are shown in Fig. 9. Black areas can be observed in the corners of the DantecDynamics iNanoSense MK7 camera. This is a result of the intensifier not covering the full sensor domain. PDF's of the images shown in Fig. 9 are provided in Fig. 10 (the entire images were considered).

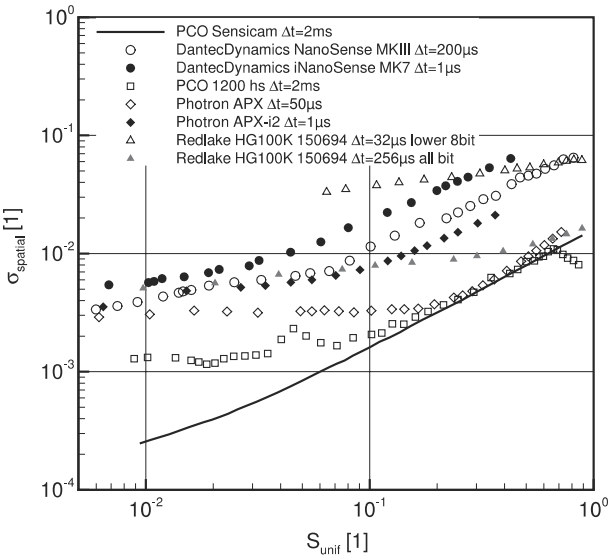


Fig. 7 Dependence of σ_{spatial} on the signal S_{unif}

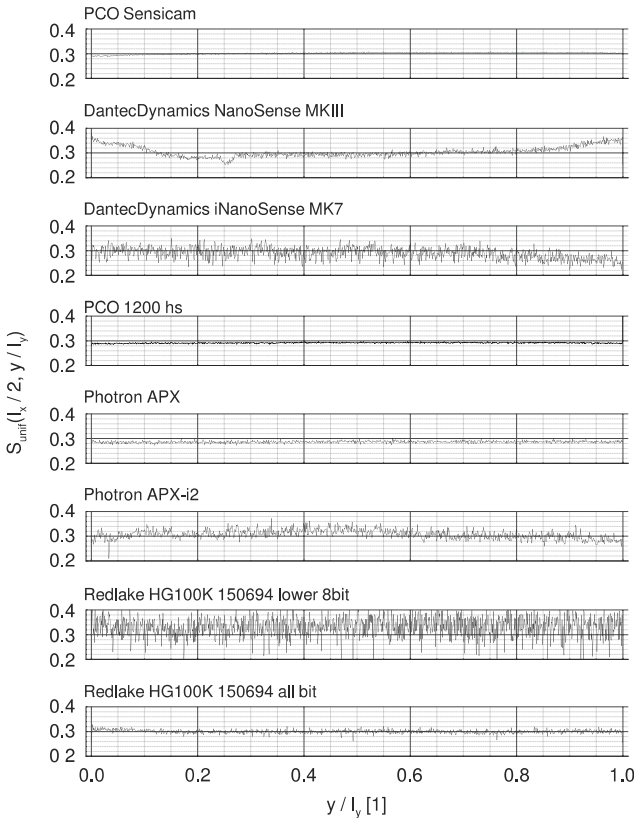


Fig. 8 Lineplot at $x = I_x/2$ ($S_{\text{unif}} \approx 0.3$)

It can be seen that the peak width of the APX-i2 is more narrow than the peak width of the iNanoSense MK7 and the shape is more Gaussian like. This indicates the APX-i2 has a slightly better image uniformity which is in agreement with Fig. 7.

4.4 Temporal variation of the mean gray value

In Fig. 11, the mean gray value of a rectangular image subsection as a function of 20 consecutive images is shown. For the PCO Sensicam and the Photron APX, no variation with time can be observed. The Photron APX-i2 shows a strong variation with time in the mean gray value between odd and even images. This must be due to the intensifier because the non-intensified APX does not show this effect.

5 Effect of pixel size and lens properties

The pixel size has a large influence on the results shown in the previous section. For real experiments, the projection of the pixel in physical space must be constant for transferring the results. A sketch with the notations for the following investigation is given in

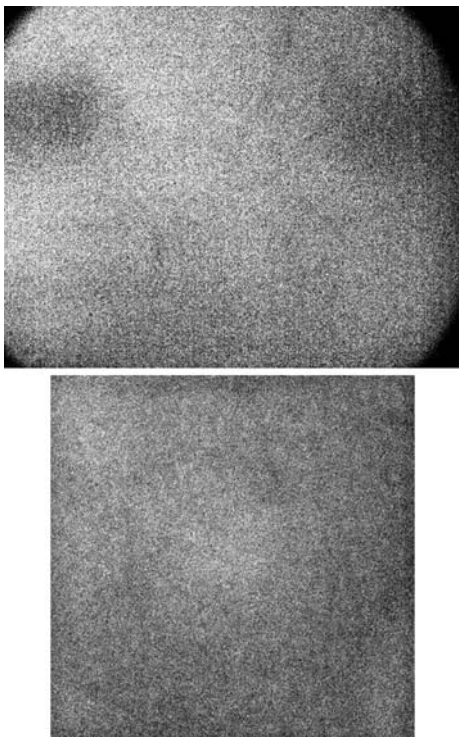


Fig. 9 Images with homogeneous illumination (same color scale). DantecDynamics iNanoSense MK7 (upper image) and Photron APX-i2 (lower image). Dark images have been subtracted. The black regions in the upper image are not covered by the intensifier, so no signal can be registered

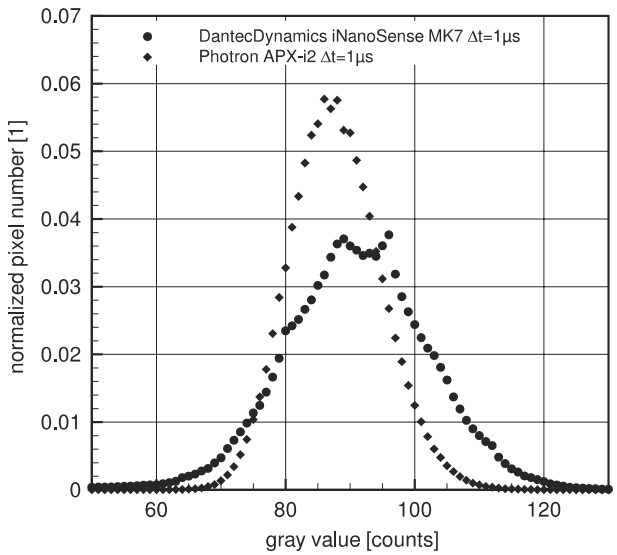


Fig. 10 PDF's of the image gray levels shown in Figure 9

Fig. 12. When a quadratic reference pixel with a size of $l_{\mathrm{ref}} \times l_{\mathrm{ref}}$ and a fill factor (ratio of the light sensitive area to the total area) of 1 is assumed, the light sensitive area is $A_{\mathrm{ref}} = l_{\mathrm{ref}}^2$. It is trivial that the number of

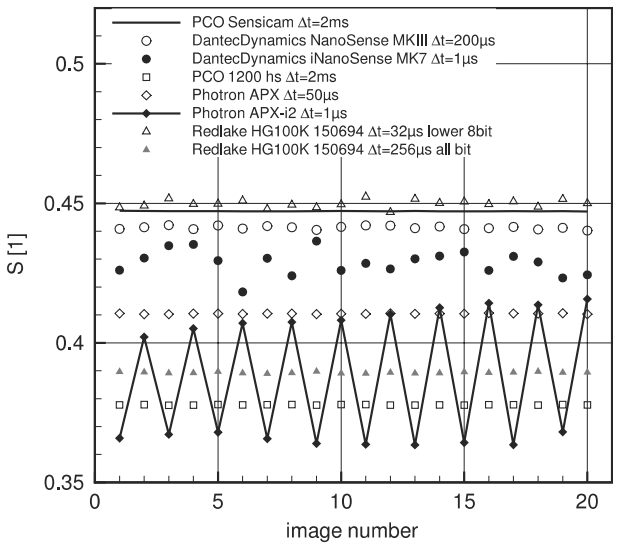


Fig. 11 Dependence of the signal, S, on time (lines for APX-i2 added for clarity)

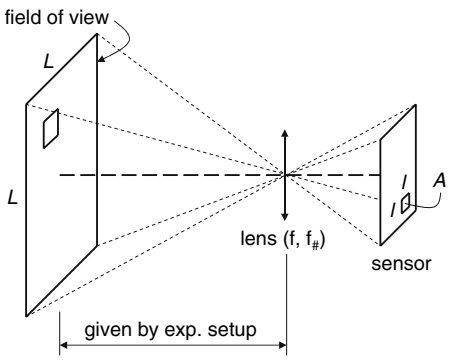


Fig. 12 Notations and setup for the investigation of pixel size and lens properties

photons impinging on a pixel increases linearly with the pixel area. If the quantum efficiency of the pixel is 1, such that all photons are registered by the sensor, the signal, S, increases linearly with the pixel area as well. The total noise is composed of three parts: 1. The photon noise which is proportional to $\sqrt{S}$ and thus $\sqrt{A}$. 2. The read-out noise which is independent from S or A. 3. The amplifier noise which is independent from S or A. From this behavior of the noise it follows the well known fact that larger pixel size leads to a higher signal-to-noise ratio.

Consider an experimental setup where the dimensions of a rectangular field of view are $L \times L$. When assuming the distance from the lens to the object is constant for the given setup, one must apply a lens with the focal length

$$f = f_{\mathrm{ref}} \cdot \frac{l}{l_{\mathrm{ref}}} \tag{8}$$

to get the same field of view with the pixels of size $l \times l$ as using the reference configuration with the focal length f_{ref} and a pixel size of $l_{\mathrm{ref}} \times l_{\mathrm{ref}}$. For example, if the pixel size, l, is twice the reference pixel size, l_{ref}, then the focal length, f, must be twice the reference focal length, f_{ref}. The number of incoming photons, P, depends on the aperture of the lens and is proportional to

$$P \sim \frac{\pi}{4}\left(f/f_{\#}\right)^2. \tag{9}$$

The ratio with the reference configuration is calculated by

$$\frac{P}{P_{\mathrm{ref}}} = \frac{l^2}{l_{\mathrm{ref}}^2}\frac{f_{\#,\mathrm{ref}}^2}{f_{\#}^2} \tag{10}$$

under consideration of Eq. 8. From Eq. 10, it follows that the signal (number of photons) increases proportionally to l^2 / l_{ref}^2 or A / A_{ref}, assuming the same numerical aperture for both configurations. This is in agreement with the setup which was applied for the experiments presented in this paper because the signal also increases proportionally to A / A_{ref} if no lens is used.

In real experiments, one often has problems with low light intensities (e.g., limited laser power) and as a result the aperture must be fully opened. As shown in Eq. 8, larger pixels require a larger focal length f. In general, the larger the focal length is, the larger is the minimum $f_{\#}$. For example, lenses with a focal length of $f = 50$ mm are available with an $f_{\#}$ of 1.4 (Nikon AF 50 mm/1.4D). If the sensor has a pixel size which is twice the pixel size in the $f = 50$ mm case, a focal length of $f = 100$ mm must be used to get the same field of view. A lens which can be used and which is comparable to the 50 mm lens has a focal length of $f = 105$ mm but a $f_{\#}$ of only 2.0 (Nikon AF DC 105 mm/2D). By means of Eq. 10 one can see that the relative signal increases by a factor of approximately 2 and not by a factor of approximately 4 (assuming the same numerical apertures, $f_{\#} = f_{\#,\,\mathrm{ref}}$).

The example shows how the pixel size will have an influence on the results for particular experimental setups. If there is enough light and the $f_{\#}$ is not the limiting factor, the results from the camera tests presented here are directly applicable to experiments. Otherwise, the dependence of the signal on the pixel size and the $f_{\#}$ must be considered according to Fig. 10.

In addition, other properties have to be considered such as the modular transfer function (MTF) of the lens. Most lenses have comparatively poor MTF at wide-open apertures which leads to decreasing intensity with increasing distance from the image center. However, for many applications a large pixel size is advantageous for getting a high SNR. Conversely, some measurement techniques like PIV require small pixel sizes in order to get particle images with a diameter of at least 2 px.

6 Conclusion and outlook

The comparison of the digital cameras shows:

- State-of-the-art CMOS cameras have a good image quality. However, the image quality of state-of-the-art CCD cameras is still better. Thus, for high precision measurements a CCD camera should be applied.
- Intensified CMOS cameras further reduce the image quality and spatial resolution. However, their high sensitivities allow measurements at low illuminations with moderate signal-to-noise ratios.
- For time resolved data acquisition, a CMOS camera without an intensifier is the best choice as long as the signal strength is acceptable.

In spite of these points, a recommendation for a certain camera will not be given because each application has a certain requirement on the camera. To capture high speed events, a CMOS camera must be applied to get a sufficient frame rate. When the signal is extremely weak, an intensified camera can be used or the signal strength must be improved in some way. In the case of time resolved PIV, for instance, this can be achieved by increasing the light intensity for the illumination of the tracer particles. Increasing the energy by a factor of two is possible but the price is quite high. An intensified camera can achieve a factor of ten with less cost. On the other hand, for multiple camera arrangements, it may be more economical to invest in a more powerful laser and non-intensified cameras to reduce the total purchase cost and measurement noise. The conventional PIV, for instance, requires double frame cameras with high sensitivity and small pixels in order to avoid the peak-locking effect. For the pressure sensitive paint (PSP) technique, cameras with a large dynamic range and low noise are required.

This experimental investigation shows the strong difference between state-of-the-art imaging sensors. However, the results may help to select the most appropriate device for a given application.

Acknowledgments This research has been partially supported by the German Research Foundation (DFG) in the priority program 1147 ''Bildgebende Messverfahren für die Strömungsanalyse''. The authors acknowledge the support of Dr. N. Andersen from Dantec Dynamics for the operation of the DantecDynamics iNanoSense MK7 camera and of Mr. C. Knieß from VKT Video Kommunikation GmbH for providing the Photron APX and APX-i2 system. Finally, the authors gratefully acknowledge the critical comments of Dr. G. Holst from PCO AG.

References

European machine vision association (2005) 1288 EMVA standard compliant, standard for characterization and presentation of specification data for image sensors and cameras. European machine vision association, Release A1.00

Janesick JR (2001) Scientific charge-coupled devices. SPIE PRESS Monograph

Jähne B (2004) Vergleichende analyse moderner Bildsensoren für die optische Messtechnik. Sensoren und Messsysteme 2004, VDI, Düsseldorf, VDI-Berichte 1829:317–324

Strüder L, von Zanthier C (1998) Elektronische Bildwandlung. Phys Bl 54: 519-523

Theuwissen AJP (1995) Solid-state imaging with charge-coupled devices. Solid-State Science and Technology Library, Kluwer